Automated Identification of Coronal Holes from Synoptic EUV Maps

A. Hamada*, T. Asikainen, I. I. Virtanen and K. Mursula

ReSoLVE Centre of Excellence, Space Physics and Astronomy Unit, University of Oulu, Finland

*email : amr.hamada@oulu.fi

1. Introduction

- Coronal Holes (CH) are regions of open, predominantly unipolar magnetic field on the Sun. They are the source of high-speed solar wind.
- CH appear dark in solar images because coronal electron density in CH is lower than in the surrounding areas of solar corona.
- Their exact identification in solar images is challenging, because their boundaries are obscured by surrounding active regions and because they appear differently in different wavelengths.
- Here, we study synoptic maps based on EUV images from two satellite instruments:

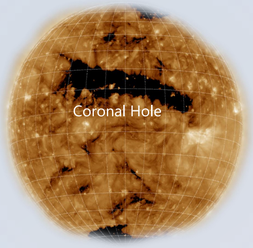

SOHO/EIT (Extreme Ultraviolet Imaging Telescope)

- Stanford Solar Observatories Group* for years 1996-2007
- Space Weather Lab at George Mason University** for years 2007-2010
- Three wavelengths 171Å, 195Å and 304Å are used here.

SDO/AIA (Atmospheric Imaging Assembly)

- Space Weather Lab at George Mason University** for years 2010-2017
- Three wavelengths: 171Å, 193Å and 304Å are used here.

- We present a new automated algorithm for identifying CHs and some first results of CH properties and their temporal evolution during the solar cycles 23 and 24.

2. Automated Coronal Hole Identification Algorithm

The algorithm is based on automatically finding the optimal image segment with the optimal size, which has **[1]** as large a contrast (C) as possible and **[2]** as low a mean intensity as possible.

These two criteria aim to ensure that the segment intensity histogram is bi-modal, consisting of two separate distributions: dark CHs and the brighter background of the quiet Sun.

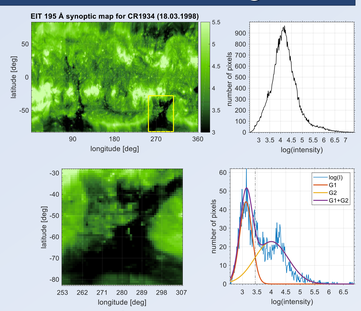

Figure 1. EIT/195Å synoptic map for CR 1934 (1998 March 18) and its intensity distribution (upper panels). The yellow box indicates the optimum segment of length $w = 55^{\circ}$, an expanded view and the intensity histogram are shown in the lower panels. The segment histogram was fit to a sum of two Gaussians shown in the lower right panel. The vertical dash line indicates CH threshold intensity.

The steps of the algorithm:

1. The image is scanned, by degree, from bottom-left corner to top-right using a square segment of variable width ($\boldsymbol{w}$).

2. For each segment we calculate RMS Contrast (C) as the standard deviation of logarithmic pixel intensities.

3. Best segment of size ($\boldsymbol{w}$) is found by maximizing the score function $\boldsymbol{R}$ defined as

$$R = \frac{C - \mu_C}{\sigma_C} - 2\frac{I - \mu_I}{\sigma_I}$$

where $\boldsymbol{\mu_C}$, $\boldsymbol{\mu_I}$, $\boldsymbol{\sigma_C}$ and $\boldsymbol{\sigma_I}$ are the mean values and the standard deviations for contrast (C) and average log intensity ($\boldsymbol{I}$) of all available image segments in the map, respectively.

4. Best segment of the whole synoptic map is found by performing steps 1-3 for segment sizes w=15...55 in 5 degree steps, and finding the segment with largest R.

5. The pixel intensity distribution of the best segment is fitted to a sum of two Gaussians G1 and G2 (see Fig. 1).

6. CH threshold Intensity is defined as the intersection between the two fitted Gaussians, and CH related pixels are identified as those with an intensity less than this value.

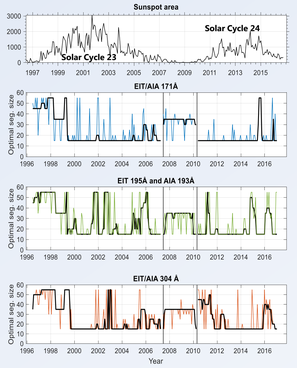

Figure 2. Variation of the optimal segment size with time for the three EIT/AIA wavelengths (171Å, 195/193Å and 304Å). The black solid lines show the 5-point running median. Vertical solid lines represent the separation between differerent data sets.

3. Synoptic Coronal Hole Maps

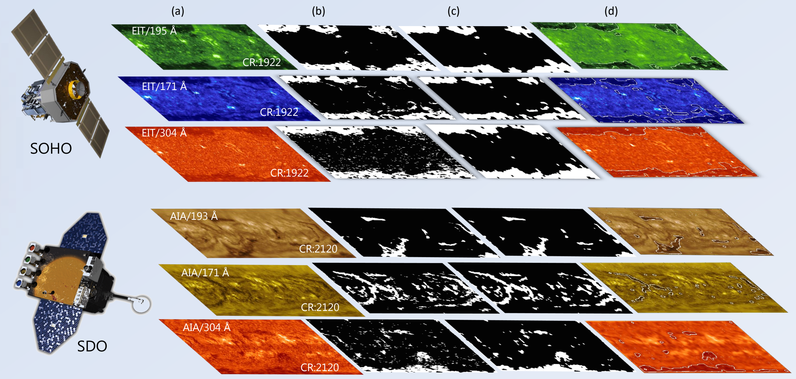

Figure 3. Example of automated CH detection for Carrington Rotations 1922 (1997 April 24) and 2120 (2012 Feb. 06) using SOHO/EIT and SDO/AIA EUV intensity synoptic maps, respectively, for **(a)** 304 Å , 171 Å and 195/193 Å. **(b)** Resulting preliminary binary map after determining the CH threshold. **(c)** Fully processed and smoothed binary map. **(d)** Edged CH areas overlaid on the EUV maps.

Filtering: The preliminary map of CH pixels (Figure 3b) often shows spurious noise, which is then filtered out (Figure 3c) using morphogical image analysis functions presented by, e.g., Michielsen & De Raedt (2011).

Magnetic polarity: Each CH boundary obtained from EUV images is superimposed with the corresponding synoptic map of the radial magnetic field obtained by the SOHO/MDI (Michelson Doppler Imager) and SDO/HMI (Helioseismic and Magnetic Imager) instruments and the relative flux imbalance $\langle B_r \rangle / \langle |B_r| \rangle$ was determined for the contoured regions.

CHs tend to favor one polarity, while filament channels (FC), which also appear dark on EUV images have a bi-polar distribution of polarities (Scholl & Habbal 2008).

CHs were differentiated from FCs by requiring that the flux imbalance for CHs is larger than 15%, i.e. $|\langle B_r \rangle / \langle |B_r| \rangle| < 0.15$.

4. Coronal Hole Evolution During Solar Cycles 23 and 24

The fractional CH area $f_{CH}(\lambda_i)$ at heliographic latitude λ_i is

$$f_{CH}(\lambda_i) = \frac{n(\lambda_i)\cos(\lambda_i)}{\sum_i N(\lambda_i)\cos(\lambda_i)}$$

$n(\lambda_i)$: The number of CH pixels at latitude λ_i

$N(\lambda_i)$: Total number of pixels with data at latitude λ.

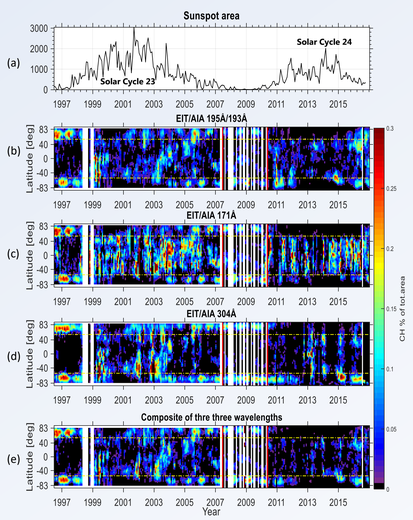

Figure 4. Fractional CH areas at different latitudes in 1996-2017. **(a)** Monthly sunspot area. **(b-d)** Fractional areas CH for 195 Å /193 Å, 171 Å and 304 Å, respectively. **(e)** Composite CH areas computed as the median of the CH maps of the three wavelengths. Horizontal yellow dashed lines at 55° latitude distinguish polar and lower-latitude zones.

- Horizontal lines at ±55° latitude are shown here to denote the division to polar and lower-latitude regions.
- Significant Polar Coronal Holes (PCH; poleward of ±55° latitude) are visible (in all three spectral lines) during the declining phases and minima of the three solar cycles.
- The yearly variation related to the changing visibility into the solar poles from Earth, the so called b_0 or vantage point effect, is seen in PCH occurrence, oppositely phased in the northern (peaks in fall) and southern (peaks in spring) hemisphere.
- All three wavelengths show CHs fairly similarly.

➔ A robust composite CH distribution (Figure 4e) is obtained as the median of the synoptic binary maps of the three wavelengths.

- Figure 5 indicates by what fraction the low latitude CHs (LLCH; within ±55° latitude) and PCHs in the northern and southern hemispheres contribute to the total CH area at different times.
- In solar minima the CH area is dominated by PCHs. In the solar maxima and early declining phase the CH area is dominated by LLCHs.

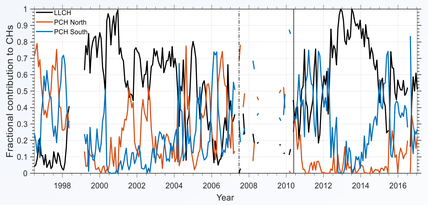

Figure 5. Fractional contribution of mid- to low-latitude CHs (LLCH) and polar CHs (PCH) in the north and south to the total CH area according to the composite CH distribution. **Black** line corresponds to LLCH, **red** line to northern PCH and **blue** line to southern PCH.

5. CH and Magnetic Field Evolution

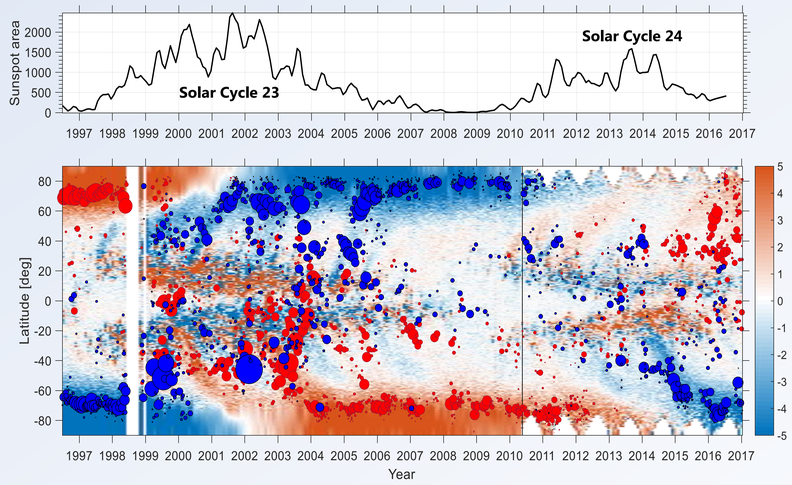

Figure 6. CH evolution through solar cycles 23 and 24. **Top panel**: total sunspot area for reference. **Bottom**: The circles depict CH as centroids with size proportional to CH size on the solar surface. The color of the circle indicates the dominant polarity of the CH (**red** is positive polarity and **blue** negative) based on the relative magnetic flux imbalance. Background color indicates the average photospheric magnetic field intensity in units of Gauss. The solid vertical line indicate the start of AIA time period.

- We identified each unique CH on the composite CH maps and approximated them as circles (centroids).
- Figure 6 shows these CH circles with size proportional to size on solar surface colored by their magnetic polarity.
- The distribution of CHs follows rather closely the evolution of the regions of unipolar magnetic field in the photosphere.
- In the ascending phase, the CHs along with unipolar regions of photospheric magnetic flux begin to rush to the poles from mid- and low latitudes (so called poleward surges of new flux), reversing the dominant polarity at high latitudes.

6. Summary and Conclusions

- We have developed an automated CH identification algorithm based on finding the threshold intensity of CHs from the best representative image segment.
- This algorithm can
  - identify CHs in different conditions during any time of the solar cycle, regardless of the change in the overall intensity or in the threshold intensity of the CH.
  - automatically adjust itself to the changing scale size of CHs and to the temporally varying intensities either naturally or due to changes in detector properties.
  - differentiate CHs from other dark features through their relative magnetic flux imbalance.
  - Produces the first ever robust composite CHs map from different wavelengths.

We found that :

- Polar CHs peak in the late declining to minimum phase of the solar cycle.
- Low-latitude CHs peak in the early declining phase of the solar cycle.
- Polar CHs are significantly affected by seasonally varying visibility into the polar regions (the b_0 effect).
- The three wavelengths show somewhat different CH evolution partly because they correspond to different heights in the solar corona.
- The extracted CH boundaries open many possibilities to study long-term variation of CH properties.

Detailed description of the work presented here can be found in the article:

Hamada, A., T. Asikainen, I.I., Virtanen and K. Mursula, Automated identification of coronal holes from synoptic EUV maps, Solar phys., in press 2018.

You can download an electronic version of this paper by scanning the QR code.

Other references:

K. Michielsen, H. De Raedt, Integral-geometry morphological image analysis, Physics Reports, Volume 347, Issue 6, July 2001, Pages 461-538, ISSN 0370-1573

Scholl, I.F. & Habbal, S.R., 2008. Automatic Detection and Classification of Coronal Holes and Filaments Based on EUV and Magnetogram Observations of the Solar Disk. Solar Physics, 248(2), pp.425–439. Available at: http://link.springer.com/10.1007/s11207-007-9075-6 [Accessed September 9, 2016].

* http://sun.stanford.edu/synop/EIT/index.html

** http://spaceweather.gmu.edu/projects/synop/EITSM.html